Electronic Transport Study of Bistable Cr@C28 Single-Molecule Device for High-Density Data Storage Applications

Proceedings of the 8th World Congress on New Technologies (NewTech'22)
Prague, Czech Republic– August 03-05, 2022
Paper No. ICNFA 138
DOI: 10.11159/icnf22.138

Electronic Transport Study of Bistable $Cr@C_{28}$ Single-Molecule Device for High-Density Data Storage Applications

Chiara Elfi Spano[1†], Fabrizio Mo[1†], Yuri Ardesi[1], Massimo Ruo Roch[1], Gianluca Piccinini[1], Mariagrazia Graziano[2]
[1]Department of Electronics and Telecommunications, Politecnico di Torino,
corso Duca degli Abruzzi 24, Torino, Italy
chiaraelfi.spano@polito.it; fabrizio.mo@polito.it;
[2]Department of Applied Science and Technology, Politecnico di Torino,
corso Duca degli Abruzzi 24, Torino, Italy
[†]These two authors contributed equally to this work.

Abstract - We investigate through *ab initio* calculation the endohedral monometallofullerene $Cr@C_{28}$ as a candidate for data storage applications. First, we study the encapsulation energy and the electronic properties of two stable states of the $Cr@C_{28}$ - namely I-$Cr@C_{28}$ and II-$Cr@C_{28}$. Then, we address the adsorption of C_{28}, I-$Cr@C_{28}$, and II-$Cr@C_{28}$ onto a gold substrate. Finally, by emulating a Scanning Tunneling Microscope (STM) break-junction experimental setup, we analyze the STM-mediated transport characteristics for the most probable adsorption configurations. We find and discuss a significant and measurable current difference between the two stable states. This outcome enables the binary encoding of the information, making the proposed device promising as a single-molecule data storage element for future high-density integrated circuits.

***Keywords*:** Endohedral Cr-fullerene, Data Storage, Endohedral Fullerenes, Nanoelectronics, Single-Molecule Electronics, Nanoscale Transport.

1. Introduction

Nowadays, the demand for continuing Moore's law of scaling, the ubiquitous paradigm of the Internet of Things, and the pervasive use of big data led to an escalation in demand for high-density data storage devices and heavily scaled integrated circuits. Current commercial technologies employ about one million atoms to store a single bit of data, and an enormous research effort is devoted to miniaturize memory elements. New strategies were proposed to fulfill this demand both at the architectural level, e.g., through the logic-in-memory paradigm [1], [2] and at the technological level, with the investigation of innovative memory materials [3], [4]. Furthermore, various attempts have been made to design and fabricate highly dense memory devices with only few atoms per bit storage, but their practical application is still limited to very low operating temperatures [5], [6].

In this scenario, among the beyond-CMOS possibilities, the molecular electronics is promising for its potentially massive scalability and the contained power dissipation [7]-[9]. However, even if several computing device prototypes were proposed over the years, there is still a lack of single-molecule devices for memory applications [10]. At the same time, Endohedral Fullerenes (EFs) have recently attracted considerable attention for their rich electronic properties that offer potential applications for information storage, and in other fields such as quantum computing processing, biomedicine (e.g., radiotherapy, MRI spectroscopy), and energy conversion [11]-[14].

EFs are fullerene cages where a variety of moieties, including ions, small molecules or metal atoms and clusters, are encapsulated through molecular surgery technique. In particular, EFs with single encapsulated metal atoms, i.e., Endohedral Monometallo Fullerenes (EMFs), were proved and synthesized [15]. Zhang *et al.* recently reported an EMF (Gd@C82) exhibiting electric polarization switching at room-temperature [16] paving the way towards practical applications of single-molecule memory devices, with the advantage of low-fabrication costs, thanks to self-assembly techniques [17], and intrinsic ultra-high integration density.

In this work, we investigate and compare the electronic structure properties of the fullerene C_{28} and its chromium (Cr) endohedral form Cr@C_{28} through *ab initio* calculation. Our results reveal a bistability of the Cr@C_{28}, required feature for binary logic states encoding. Furthermore, through an investigation of the transport properties of the two stable states, we find the two Cr@C_{28}-based Scanning Tunneling Microscope Break Junctions (STM-BJs) states exhibit a significant current difference demonstrating EMFs to be promising as single-molecule devices for data storage applications.

2. Methodology and Computational Details

The C_{28} is known to exist at room temperature in two different configurations: namely the T_d symmetry and the D_2 symmetry [18]. In T_d symmetry, all the hexagons are separated by pentagons, thus according to the Pentagons Adjacency Penalty Rule (PAPR) and, as theoretically demonstrated in [19], it is the most energetically stable. For this reason, in this work, we consider the T_d symmetry configuration reported in Fig. 1(a) (top-left). Concerning the C_{28} endohedral form encapsulating the Cr, we consider few initial guesses for the position of Cr inside the carbon cage starting from the work reported in [13], and then we optimize the geometries to permit relaxation and obtain the equilibrium positions of the Cr inside the C_{28} cage. The relaxed endohedral geometries are reported in Fig. 1(a) - middle and right ones. We refer to the two geometries as I-Cr@C_{28} (state I) and II-Cr@C_{28} (state II).

To perform the above mentioned geometry optimization calculations of the isolated C_{28}, I-Cr@C_{28}, II-Cr@C_{28} we use the *ab initio* quantum chemistry package ORCA [20] with the Density Functional Theory method (DFT), Generalized Gradient Approximation (GGA), Becke, 3-parameter, Lee-Yang-Par exchange-correlation functional (B3LYP), Triple-□-Valence-Polarized (TZVP) basis set [21], with van der Waals (vdW) correction Grimme DFT-D3 [22],[23]. Furthermore, we calculate the total energy of the isolated molecules and of the isolated Cr atom and we derive the encapsulation energy, defined as:

$$E_{enc,i} = E_{i-CrC_{28}} - (E_{C_{28}} + E_{Cr}) \quad (1)$$

where E_{Cr} is the isolated Cr atom energy, E_{C28} is the isolated C_{28} energy, and the $E_{i\text{-}CrC28}$ with *i=I, II* are the I-Cr@C_{28} and II-Cr@C_{28} energies.

We then consider the molecular junctions as created between a gold FCC (111) substrate, acting as drain electrode (D), and a gold pyramidal STM tip acting as source electrode (S) - Fig. 1(d). This configuration emulates a typical experimental setup arrangement and permits to perform calculations useful in view of a realization of the device prototypes. We thus consider the C_{28}, I-Cr@C_{28}, and II-Cr@C_{28} molecules as deposited onto the D electrode (gold substrate), and we study the most stable adsorption configurations of the fullerenes onto the gold substrate. We perform the relaxation of three geometries per fullerene, consisting of different orientations of the fullerenes themselves w.r.t. the gold substrate. For the initial guess distances between the fullerenes and the gold substrate we refer to the work reported in [24]. The first configurations we relax, that we call "geometries A", are reported in Fig. 1(b) -front view- and (c) -top view-, while the others are obtained from these ones by rotating each fullerene of +45° and +90° w.r.t. the transverse rotation axis (entering in the page of Fig 1). We refer to the latter two configurations as "geometries B" and "geometries C", respectively. Thanks to the fullerene symmetry, these three cases cover the main adsorption configurations for the C_{28}, I-Cr@C_{28}, and II-Cr@C_{28} onto the gold substrate. The relaxation calculations are done through QuantumATK [25] employing the DFT with GGA, Perdew-Burke-Ernzerhof (PBE) exchange-correlation functional, Double-□-Polarized (DZP) basis set, and vdW DFT-D3 correction. In all cases we use the LBFGS algorithm for the energy minimization until the force on each atom becomes smaller than 0.05 eV/Å. To reduce the computational time required, we account for the whole D electrode by enforcing fixed atom boundary conditions in the Au layers. The fullerenes are instead considered as rigid bodies. We then calculate the adsorption energy of the relaxed geometries from its definition:

$$E_{ads} = E_{mol/Au} - (E_{mol} + E_{Au}) \quad (2)$$

where the pedix *mol* indicates the adsorbed fullerenes, and *Au* indicates the adsorbent D electrode. To calculate $E_{mol/Au}$ we use the Counter-Poise (CP) correction for reducing the Basis Set Superposition Error (BSSE). Once the most stable

configurations for the C_{28}, I-Cr@C_{28}, and II-Cr@C_{28} adsorption onto the gold electrode are found (i.e., the ones at the minimum energy), we contact them from the top with the STM gold tip to build the STM-BJs.

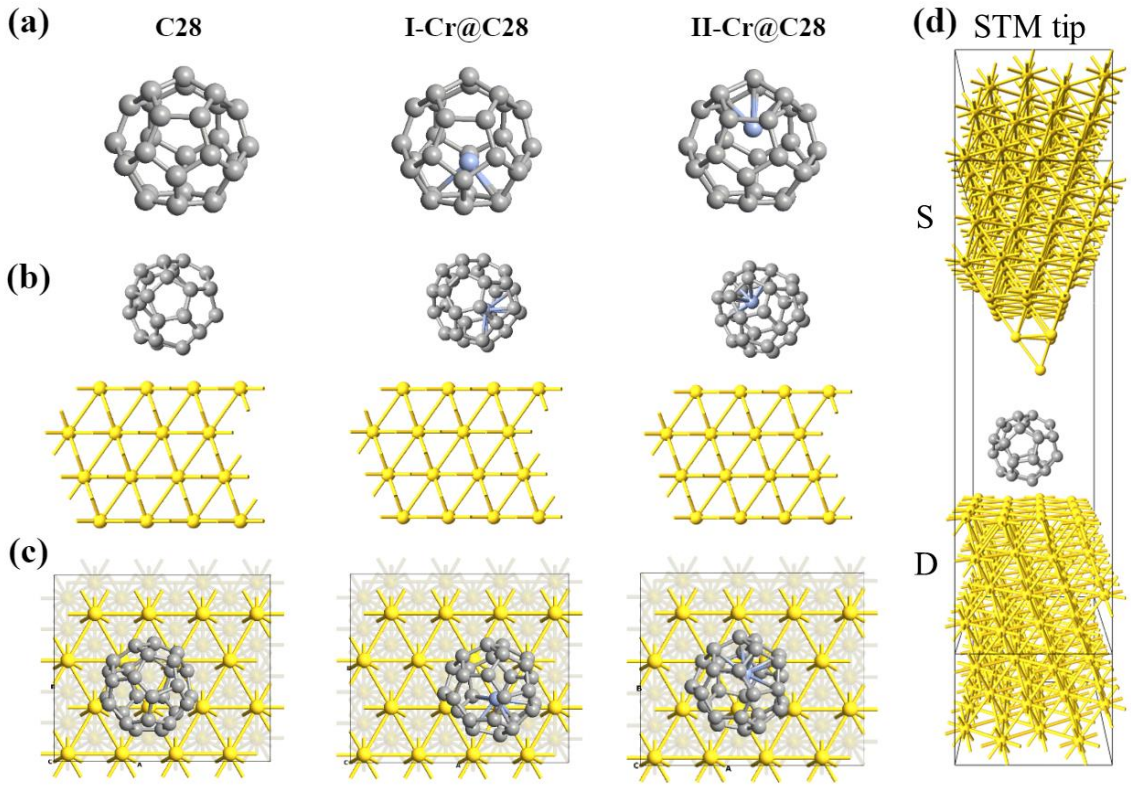

Fig. 1: (a) Molecular conformation of isolated C_{28}, I-Cr@C_{28} and II-Cr@C_{28} resulting from the geometrical optimizations; (b) front and (c) top view of the most stable adsorption geometries for C_{28}, I-Cr@C_{28} and II-Cr@C_{28} - geometries A; (d) STM-BJ configuration, the STM tip corresponds to the top electrode of the figure.

Finally, we calculate the transport of the resulting three STM-BJs self-consistently with the system electrostatics. The system electrostatics is modeled by solving the Poisson's equation using the conjugate gradient method and with periodic boundary conditions in the transverse directions to account for the electrode periodicity, while Dirichlet's boundary conditions are enforced in the transport direction. The DFT with GGA, PBE, DZP, and vdW DFT-D3 are used coupled with the Non-Equilibrium Green's Function (NEGF) formalism for the transport calculations. Thanks to the strong Au-C chemical bonds we consider coherent resonant tunneling regime, and we compute the drain-source current I_{DS} with the Landauer's formula:

$$I_{DS} = \frac{2e}{h}\int_{-\infty}^{+\infty} T(E,V_{DS})\,[f_S(E) - f_D(E)]\,dE \tag{3}$$

where e is the electron charge, h is the Plank constant, E is the electron energy, V_{DS} the applied voltage, f_S and f_D are the S and D Fermi-Dirac's distributions, respectively. $T(E, V_{DS})$ is the transmission function representing the electron transmission probability of the device; it is function of both the electron energy E and the applied voltage V_{DS}. Within the NEGF formalism the transmission function is calculated as [27]:

$$T(E,V_{DS}) = Tr[\Gamma_S G \Gamma_D G^{\dagger}] \tag{4}$$

$$\Gamma_{S,D} = i[\Sigma_{S,D}(E) - \Sigma_{S,D}{}^{\dagger}(E)] \quad (5)$$

$$G = [(E + i\eta)\, H - \Sigma(E)\,]^{-1} \quad (6)$$

where i is the imaginary unit, Tr is the trace operator, † indicates the complex conjugate and transposed, □ is a positive infinitesimal, H is the device (fullerene) Hamiltonian operator, G is the device Green's function, representing the quantum mechanical system impulse response, $\Sigma_{S,D}$ are the S and D contact self-energies and Σ is their sum, representing the effect of contacts on the isolated device, □$_{S,D}$ are the S and D contact broadening functions, representing the electron state mixing between the device and contacts. In all the performed simulations we consider room temperature environment, at 300 K. We quantify the current difference between the I-Cr@C_{28} and II-Cr@C_{28} states through the following relation:

$$\Delta I_{DS} = I_{DS,I-Cr@C_{28}} - I_{DS,II-Cr@C_{28}} \quad (7)$$

3. Results

Table 1 reports the total energies of the three isolated fullerenes and the encapsulation energies $E_{enc,i}$ of the two energetically stable states I-Cr@C_{28} and II-Cr@C_{28}. The reported energies are compatible with literature data [14], [26]. The obtained $E_{enc,I}$ and $E_{enc,II}$ are typical of covalent bonds, indicating that a strong chemical interaction occurs between the Cr atom and the C_{28} cage. Moreover, from a comparison of the total energies, both the I-Cr@C_{28} and II-Cr@C_{28} are more stable compared to the isolated C_{28}, thus the Cr has the effect of stabilizing the fullerene cage at room temperature (300 K). In particular, the II-Cr@C_{28} presents a lower total and encapsulation energies, being thus more stable than the I-Cr@C_{28}. In the II-Cr@C_{28} case, the Cr atom is centered on a pentagon of the C_{28} cage, that according to the PAPR is less stable w.r.t. the hexagon, to which the Cr atom is centered in the I-Cr@C_{28} state. Therefore, we relate the aforementioned greater stability of the II-Cr@C_{28} w.r.t. I-Cr@C_{28} to the Cr donor-like behavior with the neighboring pentagon face, acting as a stabilizer element. This is confirmed by the Mulliken elementary charge analysis reported in Fig. 2(a). It reports the net elementary charge that on average is present nearby atomic sites in the I-Cr@C_{28} and II-Cr@C_{28} cases. A negative value indicates a gain of electrons, while a positive value a loss of electrons. Since the Cr presents a slightly positive charge and the C_{28} cage a slightly negative one, the Cr acts as a donor of electrons and the C_{28} as an electron acceptor, as expected since Cr has a lower electronegativity w.r.t. carbon. Furthermore, since on average the Cr atom loses almost 0.6 electrons, the chemical interaction between Cr and C_{28} is confirmed to be covalent, with a fractional electron sharing between Cr and neighboring C atoms.

Table 1: Total and encapsulation energies of the considered fullerenes.

	C_{28}	I-Cr@C_{28}	II-Cr@C_{28}
Total energy (kJ/mol)	-2.798819· 10^6	-5.540795· 10^6	-5.540797· 10^6
$E_{enc,i}$ (kJ/mol)	-	-460.24	-461.85

In anticipation of the transport study and to understand if the additional electron states introduced by the Cr are localized or delocalized states, we analyze the Electron Localization Function (ELF) of I-Cr@C_{28} and II-Cr@C_{28} - Fig. 2(b). It is a measure of the electron wave function localization (normalized to 1) in proximity to a certain atomic site (0 if totally delocalized; 1 if totally localized). The presence of Cr (black atom) induces in I-Cr@C_{28} more localization in its neighboring C atoms (white atoms), w.r.t. II-Cr@C_{28} case (yellow atoms).

Therefore, the effect of Cr is to stabilize the C_{28} cage both in I-Cr@C_{28} and II-Cr@C_{28} configurations by introducing extra electron states, that are mainly localized states in the I-Cr@C_{28} configuration and delocalized in the II-Cr@C_{28} one.

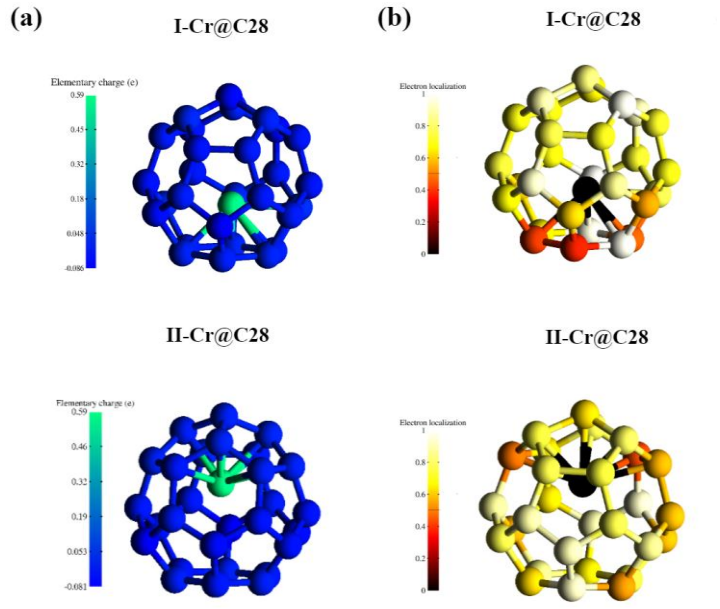

Fig. 2: (a) Mulliken elementary charge; (b) ELF distribution.

To fix the STM-BJ geometries for the transport calculations, we address the adsorption study of the fullerenes onto the gold substrates as indicated in section 2. Table 2 reports the obtained adsorption energy for the three analyzed orientations of the fullerenes w.r.t. the substrate (ref. to section 2). In all the cases (namely C_{28}, I-Cr@C_{28}, II-Cr@C_{28}), the geometries A result the most stable ones, thus we choose them for the realization of the final STM-BJ structure.

Table 2: Adsorption energies of the considered fullerenes.

E_{ads} (kJ/mol)			
Geometries	C_{28}	I-Cr@C_{28}	II-Cr@C_{28}
A	-410.2	-236.5	-266.3
B	-392.5	-223.7	-264.9
C	-373.8	-218.2	-231.6

Fig. 3(a), (b), (c) report the equilibrium Projected Density Of States (PDOS) -projected onto the fullerenes and the Cr- together with the equilibrium Transmission Spectra $T(E, V_{DS}=0)$ of the three STM-BJs. The vertical lines are the isolated fullerene energy levels. The main effect of creating a metal-molecule-metal junction is to shift in energy (Hermitian part of Σ) and broaden the energy levels (anti-Hermitian part of Σ) of the isolated molecule [27]. This effect is noticeable in all the cases when comparing the energy levels of the isolated fullerenes with the PDOS peaks. Furthermore, the broadening of the PDOS is known to be inversely proportional to the amount of time (escaping time) required on average to move an electron from the contacts to the molecule and vice versa, through a time-energy uncertainty-like relation. Wide broadening implies short escaping times and thus a large contact-molecule delocalization that permits electrons to easily move from/to contact to/from the molecule.

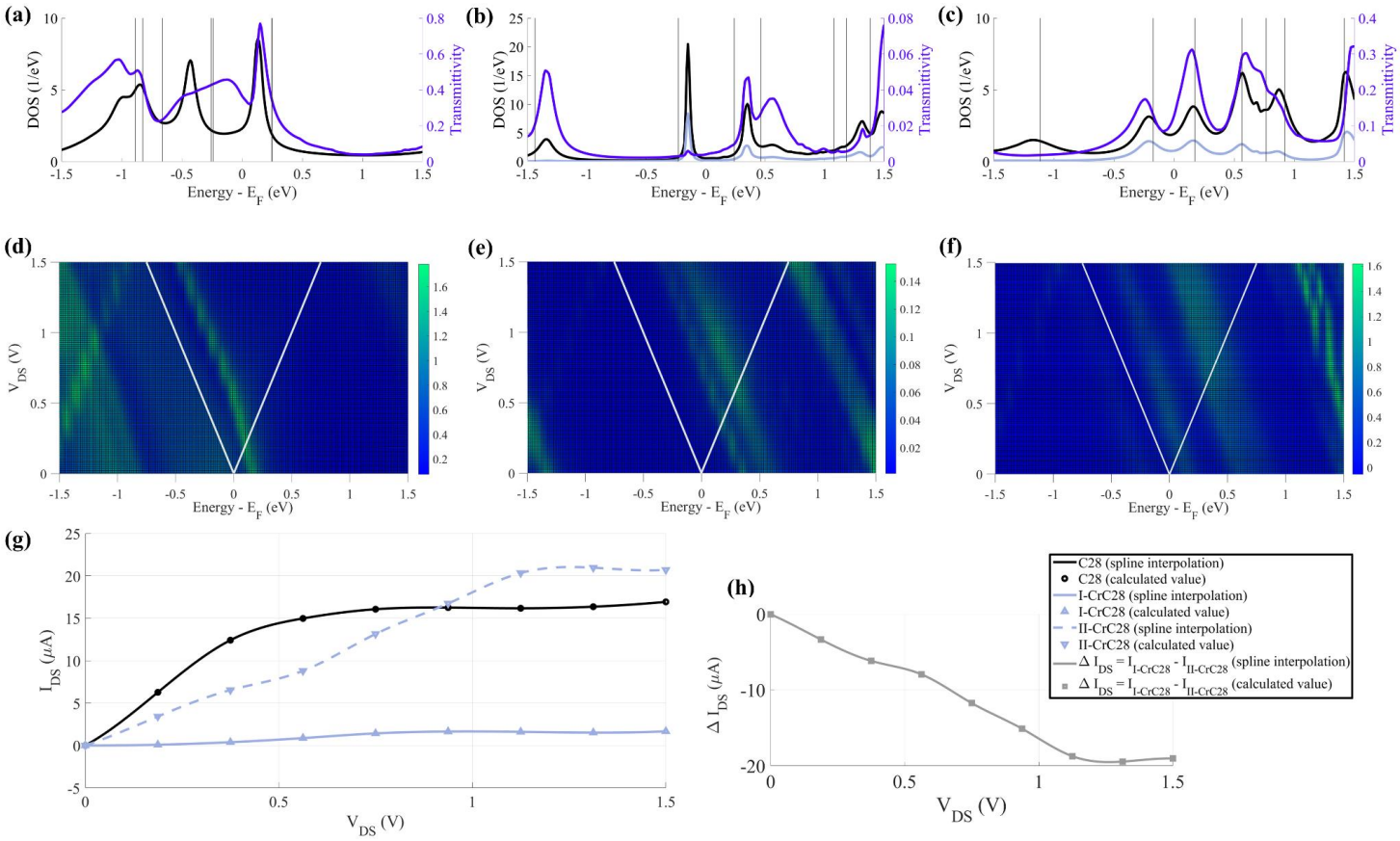

Fig. 3: Equilibrium PDOS (black: projection onto the C_{28} cage, light gray: projection onto the Cr atom), and equilibrium transmission spectra *T(E, V_{DS}=0)* (blue) of the C_{28} STM-BJ (a), I-Cr@ C_{28} STM-BJ (b), II-Cr@ C_{28} STM-BJ (c), vertical lines are the isolated molecule energy levels; (d) *T(E, V_{DS})* contour diagrams for the C_{28} STM-BJ, (e) *T(E, V_{DS})* contour diagrams for the I-Cr@C_{28} STM-BJ, (f) *T(E, V_{DS})* contour diagrams for the II-Cr@C_{28} STM-BJ. The white lines are S and D Fermi levels; (g) current-voltage characteristics of the three considered junctions; (h) ΔI_{DS} between the I-Cr@C_{28} STM-BJ and the II-Cr@C_{28} STM-BJ.

The presence of the Cr influences the fullerene PDOS (black curves) by adding a significant amount of electron states (almost half of the final PDOS is derived from Cr states - light gray curves). Such extra electron states are mainly localized states in I-Cr@C_{28} as they show a small broadening of the PDOS peaks, and are mainly delocalized in the II-Cr@C_{28} case, where the PDOS peaks are more broadened. This is in agreement with the previous considerations about the ELF analysis. The equilibrium transmission spectra resemble the PDOS in all the cases. This is expected from theory since the portion of mesoscopic devices that mainly influences the transport properties is the one with lesser amount of available electron states (w.r.t the contacts), namely the molecular channel in the studied STM-BJs [27]. In I-Cr@C_{28}, it is remarkable that, even if the sharp PDOS peak suddenly below the Fermi level (0 eV in the graph) corresponds to a large number of available states, it does not significantly contribute to conduction due to its localized nature (small transmission value). Moreover, the transmissivity in I-Cr@C_{28} at all energies is around one order of magnitude lower w.r.t. the transmittivity of C_{28} and II-Cr@C_{28}, and again we relate this to the localized states introduced by Cr in I-Cr@C_{28}.
The trends are confirmed also in non-equilibrium conditions - Fig. 3(d), (e), (f). Again, the I-Cr@C_{28} presents a much lower transmittivity for all bias voltages V_{DS} w.r.t. C_{28} and II-Cr@C_{28}, and since the localized states suddenly below the Fermi energy do not significantly conduct, the I-Cr@C_{28} presents poor conduction for a V_{DS} lower than around 0.25 V, for which

the right-side peaks start conducting since they are within the S and D Fermi levels. It is interesting noticing that in all the cases the conduction mechanism is mainly LUMO-mediated.

According to Landauer's formula -Eq. (3)- the evolution of the transmission spectra with the bias voltage V_{DS} determines the I_{DS} through the integral of the transmittivity weighted by Fermi function difference. Thus, in each V_{DS} value, the great majority of the corresponding I_{DS} is dictated by the transmission peaks within the two contact Fermi levels. Fig. 3(g) reports the current-voltage characteristics of the three STM-BJs. As expected from previous considerations, the I_{DS} of C_{28} and II-Cr@C_{28} are comparable and both greater than the I-Cr@C_{28} one.

By comparing the computed currents with the *T(E, V_{DS})* -Fig. 3(d), (e), (f)- it is expected a current saturation for the C_{28} at $V_{DS} \cong 0.3$ V because no additional transmission peaks enter within the contact Fermi levels above this V_{DS} value. A similar situation is expected for the II-Cr@C_{28} at V_{DS} above 0.8 V. Nevertheless, the Fermi function "tails" induce the full I_{DS} saturation for slightly greater V_{DS}, namely 0.5 V and 1.1 V for the C_{28} and the II-Cr@C_{28} respectively, because of the presence of additional occupied electron states at the S and free states at the D - Fig. 3(g)-, thus saturating the Landauer's integral for larger V_{DS} values.

Fig. 3(h) reports the current difference ΔI_{DS} between the I-Cr@C_{28} and II-Cr@C_{28} STM-BJs. Interestingly, the two states present very different I_{DS} values with a maximum ΔI_{DS} of almost 20 μA in magnitude. Such a distinguishable current difference between the two stable states is easily detectable, making the investigated endohedral monometallo fullerene Cr@C_{28} an extremely promising device for future data storage applications, with the considerable advantage of intrinsic miniaturization.

4. Conclusion

Thanks to molecular surgery technique, EMFs are now a reality. They have been demonstrated to exhibit plentiful of electronic properties, making them attractive for a variety of applications. In this paper, we consider the C_{28}, the smallest stable fullerene in nature, and one of its endohedral forms, the Cr@C_{28}, consisting of a single encapsulated metal atom of Cr. We find two energetically stable states of Cr@C_{28}, namely I-Cr@C_{28} and II-Cr@C_{28}, thus revealing a bistability feature essential for binary data encoding. From the study of the electron properties of the two different states we show the Cr binds to the fullerene through covalent bonds to act as structure stabilizer and as electron donor, and furthermore it introduces localized states in I-Cr@C_{28} while non-localized states in II-Cr@C_{28}. Then, we study the adsorption of the Cr@C_{28}, I-Cr@C_{28} and II-Cr@C_{28} onto a gold substrate and by selecting the most stable ones we build the STM-BJ arrangements of the three different configurations. By analyzing the transport properties of the Cr@C_{28}, I-Cr@C_{28} and II-Cr@C_{28} and by relating the findings to their electronic properties, we find that the localized nature of the Cr states in I-Cr@C_{28} hampers the transport and leads to a lower current. The current difference of 20 μA in the two states at 1 V makes possible a robust detection of logic states, i.e., a memory reading operation.

Our results motivate future works on the investigation of the transition energy between the I-Cr@C_{28} and II-Cr@C_{28} states. Once known, it would permit the determination of the gate voltage value to be applied in order to make the endohedral fullerene switching between the two stable states and permitting a writing operation of the memory cell.

References

[1] Santoro, G., Turvani, G., and Graziano, M., "New Logic-In-Memory Paradigms: An Architectural and Technological Perspective", *Micromachines, vol. 10(6)*, 2019.

[2] Zhang, Wei, Riccardo Mazzarello, Matthias Wuttig and Evan Ma. "Designing crystallization in phase-change materials for universal memory and neuro-inspired computing.", *Nature Reviews Materials*, vol. 4, 150-168, 2019.

[3] Zhou, L., Mao, J., Ren, Y., Han, S.-T., Roy, V. A. L., and Zhou, Y., "Recent Advances of Flexible Data Storage Devices Based on Organic Nanoscaled Materials", *Small*, vol. 14, 1703126, 2018.

[4] Sebastian Loth, Susanne Baumann, Christopher P. Lutz, D. M. Eigler, and Andreas J. Heinrich, "Bistability in Atomic-Scale Antiferromagnets", Science, vol. 335, p. 196-199, 2012.

[5] Fu-Sheng Guo, Benjamin M. Day, Yan-Cong Chen, Ming-Liang Tong, Akseli Mansikkamäki, and Richard A. Layfield, "Magnetic hysteresis up to 80 kelvin in a dysprosium metallocene single-molecule magnet", *Science*, vol. 362(6421), p. 1400-1403, 2018.
[6] A. Balliou, J. Pfleger, G. Skoulatakis, S. Kazim, J. Rakusan, S. Kennou, and N. Glezos, "Programmable molecular-nanoparticle multi-junction networks for logic operations," in *Proceedings of the 14th IEEE/ACM International Symposium on Nanoscale Architectures*, Association for Computing Machinery, 2018, p. 37–43.
[7] F. Mo, C. E. Spano, Y. Ardesi, G. Piccinini and M. Graziano, "Beyond-CMOS Artificial Neuron: A Simulation- Based Exploration of the Molecular-FET", *IEEE Transactions on Nanotechnology*, vol. 20, pp. 903-911, 2021.
[8] Cairo Fabrizio, Giovanna Turvani, Fabrizio Riente, Marco Vacca, Stephan Breitkreutz-v. Gamm, Markus Becherer, Maurizio Graziano and Maurizio Zamboni. "Out-of-plane NML modeling and architectural exploration." *2015 IEEE 15th International Conference on Nanotechnology* (IEEE-NANO), 1037-1040, 2015.
[9] G. Beretta, Y. Ardesi, M. Graziano and G. Piccinini, "Multi-Molecule Field-Coupled Nanocomputing for the Implementation of a Neuron", in IEEE Transactions on Nanotechnology, vol. 21, pp. 52-59, 2022.
[10] Fu, H., Zhu, X., Li, P., Li, M., Yang, L., Jia, C., and Guo, X., "Recent progress in single-molecule transistors: their designs, mechanisms and applications", *J. Mater. Chem. C*, vol. *10*, p. *2375-2389*, 2022.
[11] Adam Jaroš, Esmaeil Farajpour Bonab, Michal Straka, and Cina Foroutan-Nejad, "Fullerene-Based Switching Molecular Diodes Controlled by Oriented External Electric Fields", *Journal of the American Chemical Society*, vol. 141 (50), p. 19644-19654, 2019.
[12] Harneit, W., "Fullerene-based electron-spin quantum computer", *Phys. Rev. A*, vol. 65, p. 032322, 2002.
[13] Kato, H., Kanazawa, Y., Okumura, M., Taninaka, A., Yokawa, T., and Shinohara, H., "Lanthanoid Endohedral Metallofullerenols for MRI Contrast Agents", *Journal of the American Chemical Society*, 125(14), 4391-4397, 2003.
[14] Li, J., and Wu, R., "Ferroelectrics and photovoltaics in endohedral fullerenes-based van der Waals heterostructures", *Applied Physics Letters*, vol. 120(2), p. 023301, 2022.
[15] Murata, M., Murata, Y., & Komatsu, K., "Surgery of fullerenes.", *Chemical Communications*, vol. 46, 6083–6094, 2008.
[16] Zhang, Kangkang, Cong Wang, Minhao Zhang, Zhanbin Bai, Fang-Fang Xie, Yuan-Zhi Tan, Yilv Guo, Kuo-Juei Hu , Lu Cao, Shuai Zhang, Xuecou Tu, Danfeng Pan, Lin Kang, Jian Chen, Peiheng Wu, Xuefeng Wang, Jinlan Wang, Junming Liu, You Song, Guanghou Wang, Fengqi Song, Wei Ji, Su-Yuan Xie, Su-Fei Shi, Mark A. Reed and Baigeng Wang, "A Gd@C82 Single-Molecule Electret". *Nature Nanotechnology*, vol. 15, n. 12, 1019–24, 2020.
[17] Whitesides, G., and Boncheva, M., "Beyond molecules: Self-assembly of mesoscopic and macroscopic components", Proceedings of the National Academy of Sciences, vol. 99(8), p. 4769–4774, 2002.
[18] Jan M.L. Martin, "C_{28}: the smallest stable fullerene?", *Chemical Physics Letters*, vol. 255(1), p. 1-6, 1996.
[19] Stefan Portmann, John M Galbraith, Henry F Schaefer, Gustavo E Scuseria, and Hans Peter Lüthi, "Some new structures of C_{28}", *Chemical Physics Letters*, vol. 301(1), p. 98-104, 1999.
[20] Neese, F., "The ORCA program system", *WIREs Computational Molecular Science*, vol. 2(1), p. 73-78, 2012.
[21] F. Weigend and R. Ahlrichs, "Balanced basis sets of split valence, triple zeta valence and quadruple zeta valence quality for H to Rn: Design and assessment of accuracy", *Phys. Chem. Phys.* , vol. 7, p. 3297, 2005.
[22] S.Grimme, J.Antony, S.Ehrlich and H.Krieg, "A consistent and accurate ab initio parametrization of density functional dispersion correction (DFT-D) for the 94 elements H-Pu", *J.Chem.Phys.* vol. 132, p. 154104, 2010.
[23] S.Grimme, S.Ehrlich, and L.Goerigk, "Effect of the damping function in dispersion corrected density functional theory", *J Comput Chem*, vol. 32, p. 1456–1465, 2011.
[24] Xu K, Yang T, Feng Y, Ruan X, Liu Z, Liang G, Wang X. "Endohedral Fullerene Fe@C_{28} Adsorbed on Au(111) Surface as a High-Efficiency Spin Filter: A Theoretical Study". *Nanomaterials*, vol. 8, p. 1068, 2019.
[25] Søren Smidstrup, Troels Markussen, Pieter Vancraeyveld, Jess Wellendorff, Julian Schneider, Tue Gunst, Brecht Verstichel, Daniele Stradi, Umberto Martinez, Anders Blom, Mads Brandbyge, and Kurt Stokbro, "QuantumATK: an integrated platform of electronic and atomic-scale modelling tools", *Journal of Physics: Condensed Matter*, vol. 32(1), p. 015901, 2019.

[26] Dunk, P. W., Kaiser, N. K., Mulet-Gas, M., Rodríguez-Fortea, A., Poblet, J. M., Shinohara, H, and Kroto, H. W., "The Smallest Stable Fullerene, M@C_{28} (M = Ti, Zr, U): Stabilization and Growth from Carbon Vapor.", *Journal of the American Chemical Society*, vol. 134(22), p. 9380–9389, 2012.
[27] Datta, S., Quantum Transport: Atom to Transistor. Cambridge University Press, 2005.